Dilepton and photon emission rates from a hadronic gas. III

C.-H. Lee,[1] H. Yamagishi,[2] and I. Zahed[1]
[1]*Department of Physics & Astronomy, SUNY at Stony Brook, Stony Brook, New York 11794*
[2]*4 Chome 11-16-502, Shimomeguro, Meguro, Tokyo 153, Japan*
(Received 26 June 1998)

We extend our early analyses of the dilepton and photon emission rates from a hadronic gas to account for strange mesons using a density expansion. The emission rates are reduced to vacuum correlation functions using three-flavor chiral reduction formulas, and the latter are assessed in terms of empirical data. Using a fireball, we compare our results to the low and intermediate mass dilepton data available from CERN. Our results suggest that a baryon free hadronic gas does not account for the excess of low mass dielectrons observed at CERES but does well in accounting for the intermediate dimuons at HELIOS. The same observations apply to the recent low and high p_t dielectron rates from CERES. [S0556-2813(98)04411-2]

PACS number(s): 25.75.Dw, 12.38.Lg, 11.30.Rd, 11.40.Ha

I. INTRODUCTION

The latest experiments at the CERN SPS [1] machine have revealed a sizable enhancement of low mass dileptons above the two-pion threshold, triggering a number of theoretical investigations [2–6]. A somewhat smaller enhancement was also noticed in the intermediate mass region around the phi in both dielectron (CERES) and dimuon (HELIOS) experiments [1,7]. This region requires a strangeness assessment of the emission rates. An example is the recent analysis by Li and Gale [8].

In a recent series of investigations we have assessed the dilepton and emission rates emanating from a hadronic gas without strangeness using general principles [3,4]. We have found that the current low mass dilepton enhancement can only be accounted for by allowing for a sizable nucleon density [4]. It is important to stress that our construction is not a model. It relies on the strictures of broken chiral symmetry, unitarity, and data. Most model calculations should agree with our analysis to leading order in the pion and nucleon densities, an example being the comparison by Gale for the baryon-free rates [9].

The aim of the present work is to extend our baryon-free analysis to the strangeness sector, to account for strange mesons in the hadronic gas. Our results will borrow on the extension of the chiral reduction formulas to QCD with three flavors [10]. To leading order in the meson densities, the emission rates in the hadronic gas involve forward scattering amplitudes of real (photon) and virtual (dilepton) photons, which behavior is constrained by data mostly from electroproduction and photon-fusion reactions. By including strangeness we aim at evaluating the emission rates in the intermediate mass region around the phi. Throughout we will not consider baryons.

The structure of the paper is as follows: In Sec. II, we derive the emission rates for a baryon-free hadronic gas to leading order in the final meson densities including strange mesons. In Sec. III, we discuss the relevance of the various contributions and introduce the pertinent spectral functions. In Sec. IV, we discuss the integrated dielectron and photon emission rates. In Sec. V, we use a fireball scenario to account for our time-evolved rates in comparison to current CERES and HELIOS data. In Sec. VI, we discuss the current p_t spectrum of CERES data. Our conclusions are summarized in Sec. VII.

II. DILEPTON RATES

In a hadronic gas in thermal equilibrium, the rate $\mathbf{R}$ of dileptons produced in a unit four-volume is directly related to the electromagnetic current-current correlation function [11,12]. For massive dileptons $m_{1,2}$ with momenta $p_{1,2}$, the rate per unit invariant momentum $q=p_1+p_2$ is

$$\frac{d\mathbf{R}}{d^4q}=-\frac{\alpha^2}{6\pi^3q^2}\left(1+\frac{2m_l^2}{q^2}\right)\left(1-\frac{4m_l^2}{q^2}\right)^{1/2}\mathbf{W}(q), \quad (1)$$

where $\alpha=e^2/4\pi$ is the fine structure constant, and

$$\mathbf{W}(q)=\int d^4x\ e^{-iq\cdot x}\mathrm{Tr}[e^{-(\mathbf{H}-\mathbf{F})/T}\mathbf{J}^\mu(x)\mathbf{J}_\mu(0)]$$
$$=\frac{2}{1+e^{q^0/T}}\mathrm{Im}\mathbf{W}^F(q). \quad (2)$$

Here $e\mathbf{J}_\mu$ is the hadronic part of the electromagnetic current, $\mathbf{H}$ is the hadronic Hamiltonian, $\mathbf{F}$ is free energy, T is the temperature, and $\mathbf{W}^F(q)$ is

$$\mathbf{W}^F(q)=i\int d^4x\ e^{iq\cdot x}\mathrm{Tr}[e^{-(\mathbf{H}-\mathbf{F})/T}T^\star(\mathbf{J}^\mu(x)\mathbf{J}_\mu(0))]$$
$$=i\int d^4x\ e^{iq\cdot x}\langle 0|T^\star(\mathbf{J}^\mu(x)\mathbf{J}_\mu(0))|0\rangle$$
$$+\sum_a i\int\frac{n^a(\omega_k^a)}{2\omega_k^a}\int d^4x\ e^{iq\cdot x}\langle\pi_{in}^a(k)|$$
$$\times T^\star(\mathbf{J}^\mu(x)\mathbf{J}_\mu(0))|\pi_{in}^a(k)\rangle_{\mathrm{con}}+\cdots, \quad (3)$$

where the sum is over physical mesons including strange ones. For temperatures $T \leqslant m_\pi$ the first two terms in Eq. (3) are dominant. The first term relates to the vacuum current-current correlator and captures the essentials of the resonance gas model. It follows from e^+e^- annihilation data. The second term is the first correction to the resonance gas model resulting from one meson in the final state. Two- and higher-meson corrections in the final state can be evaluated using similar arguments [3].

Using the definition of the electromagnetic current $\mathbf{J}_\mu^{\rm em} = \overline{q}\gamma_\mu Q q = \mathbf{V}_\mu^3 + (1/\sqrt{3})\mathbf{V}_\mu^8$ and the decomposition

$$T^\star(\mathbf{J}_\mu \mathbf{J}_\nu) = T^\star(\mathbf{V}_\mu^3 \mathbf{V}_\nu^3) + \frac{1}{3} T^\star(\mathbf{V}_\mu^8 \mathbf{V}_\nu^8) + \frac{1}{\sqrt{3}} T^\star(\mathbf{V}_\mu^3 \mathbf{V}_\nu^8 + \mathbf{V}_\nu^3 \mathbf{V}_\mu^8), \tag{4}$$

we may follow [3,13] and rewrite Eq. (3) in terms of two-point correlation functions

$$\mathrm{Im}\left(i \int_y e^{-iq\cdot y} \langle 0 | \hat{\mathcal{S}} T^\star(\mathbf{V}_\mu^c(y) \mathbf{V}_\nu^d(0)) | 0 \rangle \right) = (-q^2 g_{\mu\nu} + q_\mu q_\nu) \mathrm{Im}\ \Pi_V^{cd}(q^2),$$

$$\mathrm{Im}\left(i \int_y e^{-iq\cdot y} \langle 0 | \hat{\mathcal{S}} T^\star(\mathbf{j}_{A\mu}^c(y) \mathbf{j}_{A\nu}^d(0)) | 0 \rangle \right) = (-q^2 g_{\mu\nu} + q_\mu q_\nu) \mathrm{Im}\ \Pi_A^{cd}(q^2), \tag{5}$$

and additional three- and four-point correlation functions using three-flavor chiral reduction formulas [10]. The axial-vector current $\mathbf{j}_A$ appearing in Eq. (5) is one pion reduced [3,13].

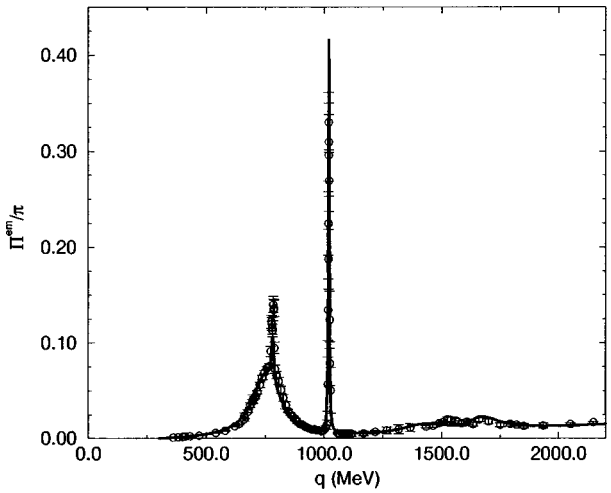

FIG. 1. Electromagnetic spectral function. See text.

With the above in mind, we have

$$\mathrm{Im}\ \mathbf{W}^F(q) = -3q^2 \mathrm{Im}\left(\Pi_V^I(q^2) + \frac{1}{4}\Pi_V^Y(q^2) \right) + \int \frac{d^3k}{(2\pi)^3} \mathbf{W}_1^F(q,k), \tag{6}$$

with $\Pi_V^I \equiv \Pi_V^{33}$ and $\Pi_V^Y \equiv \frac{4}{3}\Pi_V^{88}$. The first term is the analog of the resonance gas contribution with no chiral reduction involved. The second term is the correction to the resonance gas model resulting from one meson in the final state. Use of the on-shell three-flavor chiral reduction formulas gives, for the part involving solely the two-point correlators,

$$\begin{aligned}
\mathbf{W}_1^F(q,k) = {} & g_k^\pi \frac{12}{f_\pi^2} q^2 \mathrm{Im}\ \Pi_V^I(q^2) + g_k^K \frac{12}{f_K^2} q^2 \mathrm{Im}\left(\Pi_V^I(q^2) + \frac{3}{4}\Pi_V^Y(q^2) \right) - g_k^\pi \frac{6}{f_\pi^2}(k-q)^2 \mathrm{Im}\ \Pi_A^I((k-q)^2) \\
& - g_k^K \frac{6}{f_K^2}(k-q)^2 [\mathrm{Im}\ \Pi_A^V((k-q)^2) + \mathrm{Im}\ \Pi_A^U((k-q)^2)] - g_k^\pi \frac{6}{f_\pi^2}(k+q)^2 \mathrm{Im}\ \Pi_A^I((k+q)^2) \\
& - g_k^K \frac{6}{f_K^2}(k+q)^2 [\mathrm{Im}\ \Pi_A^V((k+q)^2) + \mathrm{Im}\ \Pi_A^U((k+q)^2)] \\
& + g_k^\pi \frac{8}{f_\pi^2}(\nu^2 - m_\pi^2 q^2) \mathrm{Re}[\tilde{\Delta}_R^\pi(k+q) + \tilde{\Delta}_R^\pi(k-q)] \mathrm{Im}\ \Pi_V^I(q^2) \\
& + g_k^K \frac{8}{f_K^2}(\nu^2 - m_K^2 q^2) \mathrm{Re}[\tilde{\Delta}_R^K(k+q) + \tilde{\Delta}_R^K(k-q)] \mathrm{Im}\left(\Pi_V^I(q^2) + \frac{3}{4}\Pi_V^Y(q^2) \right),
\end{aligned} \tag{7}$$

where $\nu = k \cdot q$. The contributions from three- and four-point correlators read

$$\mathbf{W}_1^F(q,k)=\left\{ g_k^\pi 3\sqrt{3}\frac{f_\eta m_\eta^2}{f_\pi^2}\frac{\hat m}{\hat m+2m_s}-g_k^K\sqrt{3}\frac{f_\eta m_\eta^2}{f_K^2}\frac{\hat m+m_s}{\hat m+2m_s}-g_k^\eta\frac{\sqrt{3}}{3}\frac{m_\eta^2}{f_\eta}\right\}\mathrm{Im}\,\tilde G_\sigma^8$$
$$-\frac{2}{3}\frac{K}{C}\left\{ g_k^\pi\frac{3\hat m}{f_\pi^2}+g_k^K\frac{2(\hat m+m_s)}{f_K^2}+g_k^\eta\frac{(\hat m+2m_s)}{3f_\eta^2}\right\}\mathrm{Im}\,\tilde G_\sigma^0$$
$$-g_k^a k^\beta k^\alpha (E^{-2})^{aa}\mathrm{Im}\left\{ i\int_x\int_y\int_z e^{-ik\cdot z-iq\cdot y+iq\cdot x}\langle 0|\hat{\mathcal{S}}T^\star\left[\left(\mathbf{V}^{\mu,3}(x)+\frac{1}{\sqrt{3}}\mathbf{V}^{\mu,8}(x)\right)\right.\right.$$
$$\left.\left.\times\left(\mathbf{V}_\mu^3(y)+\frac{1}{\sqrt{3}}\mathbf{V}_\mu^8(y)\right)\mathbf{j}_{A\beta}^a(z)\mathbf{j}_{A\alpha}^a(0)\right]|0\rangle\right\}$$
$$-g_k^a k^\beta\left(f^{a3l}+\frac{1}{\sqrt{3}}f^{a8l}\right)(E^{-2})^{aa}\mathrm{Im}\left([\,\delta_\alpha^\mu-(q+2k)^\mu(k+q)^\alpha\tilde\Delta_R^l(k+q)]\right.$$
$$\left.\times\left\{ i\int_y\int_z e^{-ik\cdot z-iq\cdot y}\langle 0|\hat{\mathcal{S}}T^\star\left[\left(\mathbf{V}_\mu^3(y)+\frac{1}{\sqrt{3}}\mathbf{V}_\mu^8(y)\right)\mathbf{j}_{A\beta}^a(z)\mathbf{j}_{A\alpha}^l(0)\right]|0\rangle\right\}\right)+\text{permutations}(q\to -q,k\to -k), \tag{8}$$

where the permutation applies only for the last term, and no mixing is assumed ($\Pi_V^{38}=\Pi_V^{83}=0$). The thermal meson density function g_k^a and the meson propagator $\tilde\Delta_R^a(q)$ are defined by

$$g_k^a\equiv\frac{n^a(\omega_k^a)}{2\omega_k^a}=\frac{1}{2\omega_k^a}\frac{1}{e^{\omega_k^a/T}-1},\quad \tilde\Delta_R^a(q)\equiv\frac{1}{q^2-m_a^2+i\epsilon}. \tag{9}$$

The three-point correlator $\tilde G_\sigma^h$ is given as

$$\tilde G_\sigma^h=\int_z\int_y e^{iq\cdot(z-y)}\langle 0|\hat{\mathcal{S}}T^\star\left[\left(\mathbf{V}^{\mu,3}(z)+\frac{1}{\sqrt{3}}\mathbf{V}^{\mu,8}(z)\right)\right.$$
$$\left.\times\left(\mathbf{V}_\mu^3(y)+\frac{1}{\sqrt{3}}\mathbf{V}_\mu^8(y)\right)\sigma^h(0)\right]|0\rangle. \tag{10}$$

The meson decay constants $f_K\approx 1.24 f_\pi$, $f_\eta\approx 1.32 f_\pi$, and $f_{\eta'}\approx 0.74 f_\pi$ are used [14]. The results, Eqs. (6)–(8), reduce to the two-flavor results discussed in [3]. Since they include strangeness, they can be used all the way through the phi region.

The spectral functions appearing in Eqs. (6) and (7) are related to e^+e^- annihilation data. They will be borrowed from experiment. The three- and four-point correlation functions $\mathbf{VVj}_A\mathbf{j}_A$, $\mathbf{Vj}_A\mathbf{j}_A$, and $\mathbf{VV}\sigma$ are constrained by the two-photon fusion reactions and crossing symmetry [10]. A detailed analysis of these processes shows that their contribution to our rates can be ignored for both CERES and HELIOS (2% correction). These observations confirm and extend the ones made in [3] to the three-flavor case. Hence, the two- and three-point contributions will be omitted for most of the discussion to follow.

III. SPECTRAL FUNCTIONS

In this section we derive explicit expressions for the spectral functions. The empirical information on the two-point correlators will be inserted in the rate production

TABLE I. Resonance parameters.

		$I^G(J^{PC})$	Mass (m_i)	Decay width (G_i)	Decay constant (f_i)
Π_V^I	$\rho(770)$	$1^+(1^{--})$	768.5	150.7	130.67
	$\rho(1450)$		1465	310	106.69
	$\rho(1700)$		1700	235	75.44
Π_V^Y	$\omega(782)$	$0^-(1^{--})$	781.94	8.43	46
	$\omega(1420)$		1419	174	46
	$\omega(1600)$		1649	220	46
	$\phi(1020)$	$0^-(1^{--})$	1020	4.43	79
	$\phi(1680)$		1680	150	79
Π_A^I	$a_1(1260)$	$1^-(1^{++})$	1230	400	190 (f_ρ)
Π_A^{UV}	$K_1(1270)$	$\frac{1}{2}(1^+)$	1273	90	90
	$K_1(1400)$		1402	174	90

by means of suitable spectral weights. For instance, the contribution of the nonstrange hadrons to the spectral weights is dominated by the ρ ($m_\rho=768.5$ MeV, $\Gamma_{0,\rho}=150.7$ MeV) and the a_1 ($m_{a_1}=1230$ MeV, $\Gamma_{0,a_1}=400$ MeV) resonances. For that, we will follow the arguments of [3] and use the following parametrizations:

$$\Pi_V^I(q^2)=\frac{f_\rho^2}{q^2}\frac{m_\rho^2+\gamma q^2}{m_\rho^2-q^2-im_\rho\Gamma_\rho(q^2)},$$

$$\Pi_A^I(q^2)=\frac{f_{a_1}^2}{m_{a_1}^2-q^2-im_{a_1}\Gamma_{a_1}(q^2)}, \tag{11}$$

with $f_\rho=\sqrt{2}f_\pi$ and $f_{a_1}=190$ MeV. The decay widths Γ are given by

$$\Gamma_\rho(q^2)=\theta(q^2-4m_\pi^2)\Gamma_{0,\rho}\frac{m_\rho}{\sqrt{q^2}}\left(\frac{q^2-4m_\pi^2}{m_\rho^2-4m_\pi^2}\right)^{3/2},$$

$$\Gamma_{a_1}(q^2)=\theta(q^2-9m_\pi^2)\Gamma_{0,a_1}\frac{m_{a_1}}{\sqrt{q^2}}\left(\frac{q^2-9m_\pi^2}{m_{a_1}^2-9m_\pi^2}\right)^{3/2}, \tag{12}$$

where $\theta(x)$ the Heaviside function (step function). Analogous parametrizations will be used for the strange resonances as well including the ω and ϕ in Π_V, and K_1 in Π_A. The isovector part of the spectral weight Π_V^I is dominated by the ρ and its radial excitations, while the hypercharge part Π_V^Y is dominated by the omega, the phi, and their radial excitations. In the physical basis,

$$\omega_8=\sqrt{\frac{1}{3}}\omega-\sqrt{\frac{2}{3}}\phi,\quad \Pi_V^{88}=\frac{1}{3}\Pi_V^\omega+\frac{2}{3}\Pi_V^\phi. \tag{13}$$

In Fig. 1 we show the electromagnetic spectral function $\Pi_V^{\rm em}\equiv\Pi_V^I+\frac{1}{4}\Pi_V^Y$ following from our parameters (solid curve) in comparison with the data compiled in [15].

The resonance parameters we have used are summarized in Table I [16]. The decay constants are fit to the empirical spectral weights [14]. They are all within 10% of the constituent quark model. Although the axial-vector spectral weight is not well known at large invariant mass, we observe that its numerical contribution to the dilepton emission rates is overall small.

The high energy tail of the vector spectral weight is still above the free $q\bar{q}$ threshold well through the high mass region as shown in Fig. 2 for $R_{\geqslant 3}=12\pi\,{\rm Im}\Pi(s)$ without the J/Ψ contribution. We will use the parametrization

$$\frac{0.9}{8\pi}\left[1+\tanh\left(\frac{\sqrt{q^2}-q_1}{\tilde{q}}\right)\right] \tag{14}$$

as shown by the solid line. Here $q_1=2$ GeV and $\tilde{q}=0.4$ GeV. We recall that the free $q\bar{q}$ threshold for SU(3) is

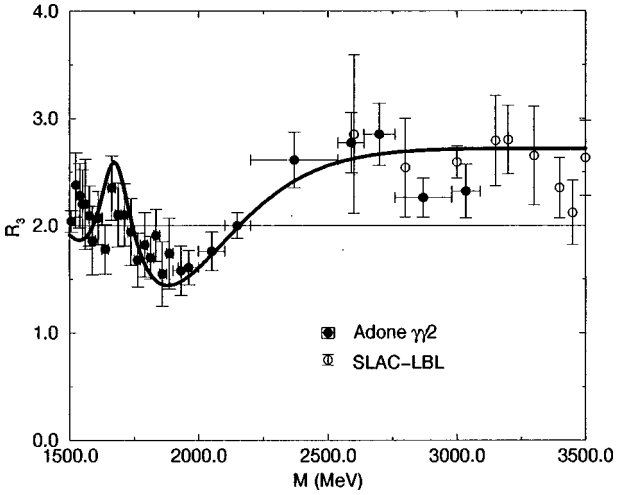

FIG. 2. $R_{\geqslant 3}$ values. Data from Adone [17] and SLAC-LBL [18].

$$R_{\geqslant 3}=\sum_i\frac{\sigma_i(\geqslant 3\pi)}{\sigma(e^+e^-\to\mu^+\mu^-)}=2\left(\frac{N_c}{2}\sum_{q=u,d,s}e_q^2\right)=2, \tag{15}$$

and underestimates the hadronic correlations by about 30% in the 2.5–3.5 GeV region. This tail is important in the emission rates as we will note in the next section. It may be interpreted as (logarithmic) corrections to the perturbative quark result by duality. Above 3.5 GeV the charm effects show up.

IV. EMISSION RATES

A. Dielectron rates

Given the two-point spectral weights, it is then straightforward to reconstruct the emission rates using Eqs. (6) and (7). The contributions, Eq. (8), are found to be numerically small and will be ignored. **R** can be reexpressed in terms of the invariant dielectron mass $M=\sqrt{q^2}$, the rapidity η, and the magnitude of the transverse momentum q_t [11]:

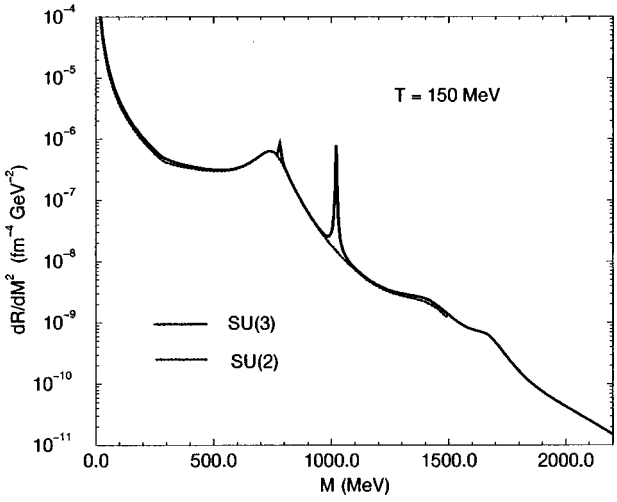

FIG. 3. Dielectron rates at $T=150$. See text.

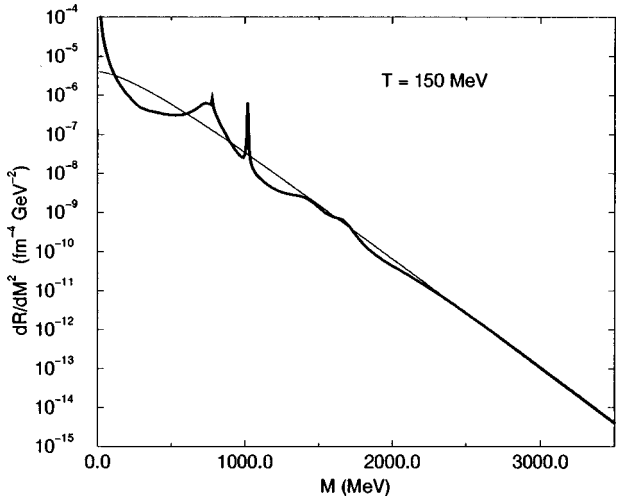

FIG. 4. Hadronic gas (bold) versus quark gas (thin). See text.

$$\frac{d\mathbf{R}}{d^2M} = \int dy \int dq_t^2 \frac{\pi}{2} \frac{d\mathbf{R}}{d^4q}(M,\eta,q_t). \tag{16}$$

In Fig. 3, we show our new three-flavor rate (solid line) in comparison to the two-flavor rate [3] (dashed line). Aside from the omega and phi which were absent in the two-flavor analysis, the results are overall consistent for $T=150$ MeV. The chiral reduction results show a substantial enhancement of the low mass dielectrons in comparison to a simple partially conserved axial-vector current (PCAC) treatment [3].

In Fig. 4 we show the rates from a hadronic gas in comparison to a free quark rate from a quark gas [19] at $T=150$ MeV. The plasma rates are large in the low mass region (more than a factor of 2), above the phi (more than a factor of 2), and around the 2 GeV region (about a factor 1/2). Surprisingly, however, the hadronic tail, Eq. (14) (e^+e^- into hadrons), still provides substantial emission strength even through the high mass region in comparison to a free quark gas at the same temperature. An enlargement of that region is shown in Fig. 5.

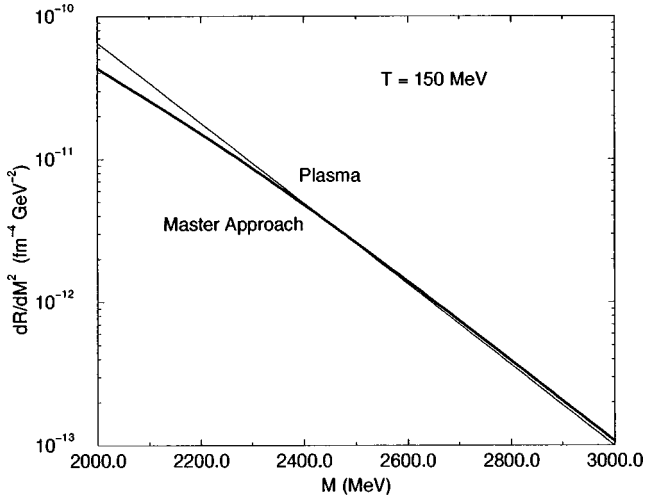

FIG. 5. Same as Fig. 4.

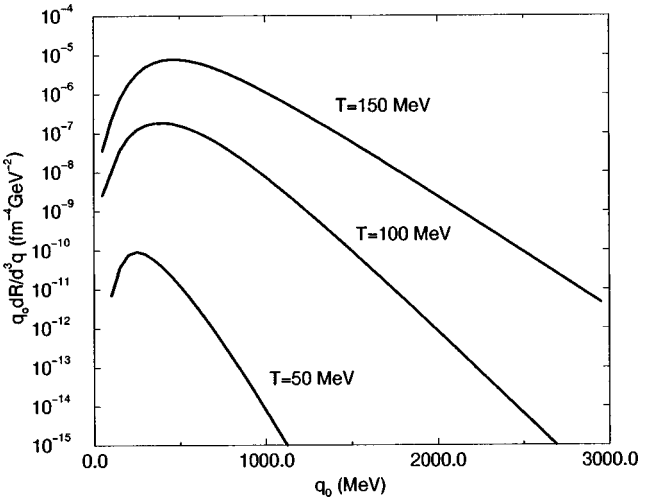

FIG. 6. The photon emission rate from a hadronic gas.

B. Photon rates

The rate for photons follows from Eq. (2) at $q^2=0$:

$$q^0 \frac{d\mathbf{R}}{d^3q} = -\frac{\alpha}{4\pi^2}\mathbf{W}(q). \tag{17}$$

Figure 6 shows the photon emission rate for $T=50,100,150$ MeV. They are overall consistent with the photon rates established for the SU(2) case [3].

V. EMISSION RATES FROM A FIREBALL

In a heavy-ion collision the electromagnetic emission occurs from various stages of the collision process. In this part, we will focus on the low and intermediate dilepton emission rates (up to 1.5 GeV). We will assume that they emanate from a simple fireball composed of a hadronic gas. The fireball will be modeled after transport codes [5], for the CERES (S-Au) and HELIOS-3 (S-W) heavy-ion collisions. In particular, the expansion will be assumed homogeneous, with a volume and temperature parametrized as [3,6]

$$V(t) = V_0\left(1+\frac{t}{t_0}\right)^3, \quad T(t) = (T_i - T_\infty)e^{-t/\tau} + T_\infty, \tag{18}$$

with $t_0 = 10$ fm/c, $T_i = 170$ MeV, $T_\infty = 110$ MeV, $\tau = 8$ fm/c, and the value of V_0 is absorbed into the overall normalization constant N_0V_0 ($=6.76\times10^{-7}$ fm^3) in Eq. (19), which is fixed by the transport results. The freeze-out time will be set to $t_{\text{f.o.}} = 10$ fm/c. Since we would like to only address the issue of a thermal gas of mesons, we will ignore the baryons, assuming their contribution at present energies to be small in the leading density approximation [4]. The mesonic fireball is more appropriate for RHIC as opposed to CERN energies.

Using Eq. (18) and the above rate, the final expression for the integrated emission rate per unit rapidity η and invariant mass M is

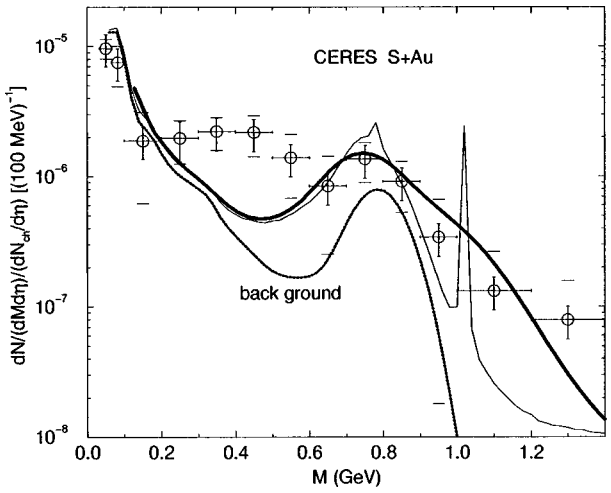

FIG. 7. Dielectron rates for the CERES S-Au experiment. See text.

$$\frac{dN/d\eta\, dM}{dN_{\rm ch}/d\eta}(M)=N_0 M\int_0^{t_{\rm f.o.}} dt\; V(t)\int \frac{d^3q}{q_0}A(q_0,q^2)\frac{d\mathbf{R}}{d^4q}. \tag{19}$$

The acceptance function $A(q_0,q^2)$ enforces the detector cut $p_t>200$ MeV, $2.1<\eta<2.65$, and $\Theta_{ee}>35$ mrad for CERES. For HELIOS-3, Eq. (19) can be used by integrating over η with the cut $m_t\geqslant 4(7-2\eta)$, $m_t\geqslant\sqrt{(2m_\mu)^2+[15/\cosh(\eta)]^2}$. The results for CERES and HELIOS-3 are summarized in Figs. 7 and 8.

The thin line in Fig. 7 is our result using only the two-point spectral weights in Eq. (19), while the thick line follows from an additional Gaussian smearing over the detector mass resolution:

$$\int_0^\infty dM'\frac{1}{\sqrt{2\pi}\sigma}\exp\left(-\frac{(M-M')^2}{2\sigma^2}\right)\frac{dN/d\eta\, dM}{dN_{\rm ch}/d\eta}(M'), \tag{20}$$

with $\sigma=0.1M$. The background (dotted line) was taken from a transport model [5,9]. The ϕ resonance is clearly visible.

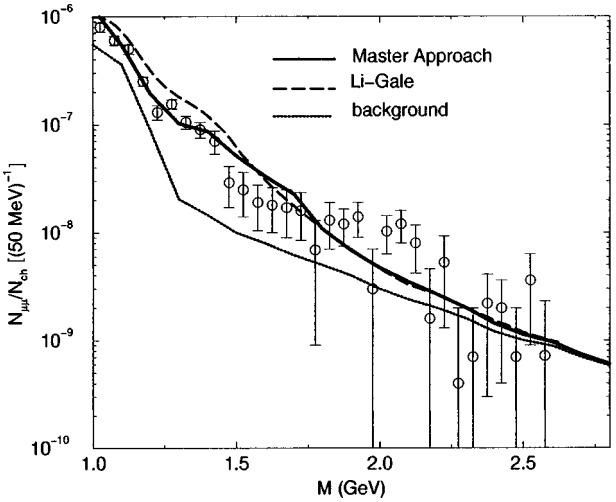

FIG. 8. Dimuon rates for the HELIOS-3 S-W experiment. See text.

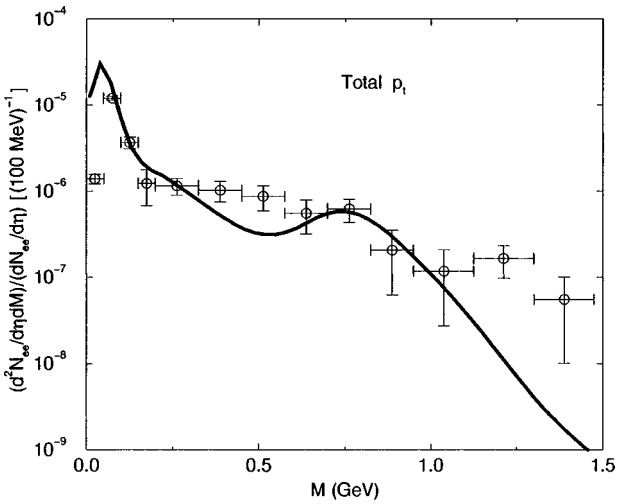

FIG. 9. Dielectron rates for the total p_t of the CERES Pb-Au experiment.

The data are from [1]. Clearly the fireball evolution and the mesonic gas do not account for the low mass dileptons. In Ref. [3], it was shown that only large nucleonic densities could account for the data to leading order in the hadronic densities.

The solid line in Fig. 8 is our three-flavor result for the HELIOS-3 experiment. The dashed curve refers to the results discussed recently by Gale [9] using effective Lagrangians and a variety of two-body reactions. Our results are in overall agreement with theirs. The dotted line is again the background contribution from the transport model [5,9]. The fair agreement of the fireball with the dimuon spectra above 1 GeV indicates that a thermal hadronic gas treatment is consistent with the data. Some enhancement in the low mass region may be achieved by adding baryons, but not enough in our leading density approximation to bring it into agreement with the data [3].

VI. CERES WITH p_t CUT

Recently, the CERES collaboration analyzed the p_t dependence of the dielectron pairs [20]. Using our mesonic

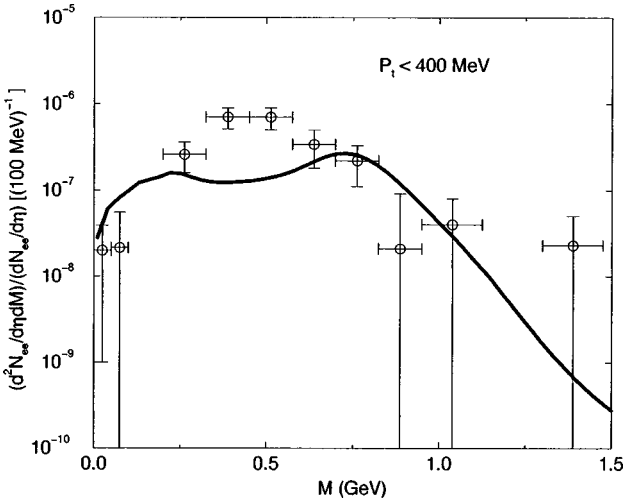

FIG. 10. Dielectron rates for low p_t of the CERES Pb-Au experiment.

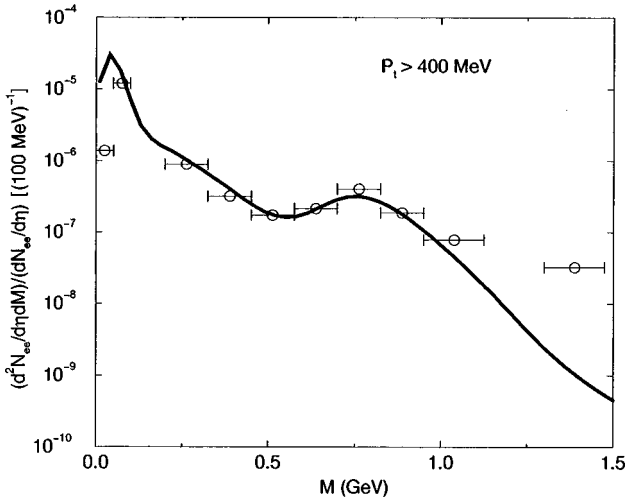

FIG. 11. Dielectron rates for high p_t of the CERES Pb-Au experiment.

rates and the fireball evolution, Eqs. (18) and (19), we show in Figs. 9 and 10 our results in comparison to data. The background contribution in our case was borrowed from transport calculations [21]. The initial temperature of the fireball is set at $T_i = 160$ MeV and the freeze-out temperature at $T_\infty = 105$ MeV for which the time scale is $t_{\text{f.o.}} = 20$ fm/c, with $\tau = 10$ fm/c and $t_0 = 10.8$ fm/c. The new normalization constant $N_0 V_0 = 3.45 \times 10^{-7}$ fm^3 is fixed by the transport results [21].

Our analysis, based on a baryon-free hadronic gas (with strange mesons), does not reproduce the low mass dielectron enhancement in both Figs. 9 and 10. Since most of the iscrepancy of the low mass enhancement comes from low p_t contribution, taking into account the large statistical and systematical errors for $M > 1.0$ GeV, we find that our high p_t spectrum is consistent with the data. In Fig. 11, the data are the differences between the mean values of the total and low p_t spectrum, and so we do not include the vertical error bars.

VII. CONCLUSIONS

We have extended the dilepton and photon emission rates from a thermalized gas of hadrons to account for strange mesons without baryons. The analysis relies on the extension of the chiral reduction formulas from SU(2) to SU(3). The hadronic gas now includes the effects from kaons, etas, and phis. As expected, only substantial changes in the rates are seen around the omega and phi regions.

In the low mass region there is a substantial enhancement due to the mixing with the axial particles, but not enough to account for the CERES data after time-evolution and detector cuts. In the intermediate mass region, there is good agreement with the HELIOS data. The baryonic effects are important in the low mass region, but not enough to account for the discrepancy seen in the Pb-Au collisions at CERN within the density expansion [3]. The large and persistent hadronic tails make the thermal mesonic emission rates comparable to the ones from a thermal gas through the intermediate mass region.

As we have indicated in the Introduction, our analysis is not based on a model. Our only assumption is that the emission rates follow from a baryon-free and dilute hadronic gas. The rest follows from symmetry and data. As such all model calculations should be in agreement with our results under these assumptions, and it is gratifying to see that the recent analysis performed by Gale [9] using reaction rates does.

The fact that the HELIOS-3 data can be explained without recourse to additional assumptions makes part of our arguments reliable. The persistent disparity in the low mass region with CERES and the newly measured p_t spectra may indicate the need for an enlargement of the original assumptions. The importance of the thermal quark gas emissivities in the 1/2 and 1 GeV regions may be indicative of some simple nonperturbative effects in the partonic phase for the temperatures considered [22]. This issue will be addressed next [19].

ACKNOWLEDGMENTS

We have benefited from several discussions with Gerry Brown, Axel Drees, Charles Gale, Guoqiang Li, Madappa Prakash, Ralf Rapp, Edward Shuryak, Heinz Sorge, and Jim Steele. This work was supported in part by the U.S. Department of Energy under Grant No. DE-FG02-88ER40388.

[1] G. Agakichiev *et al.*, Phys. Rev. Lett. **75**, 1272 (1995); Nucl. Phys. **A610**, 317c (1996).

[2] W. Cassing, W. Ehehalt, and C. M. Ko, Phys. Lett. B **363**, 35 (1995); G. Q. Li, C. M. Ko, and G. E. Brown, Phys. Rev. Lett. **75**, 4007 (1995); F. Klingl and W. Weise, Nucl. Phys. **A606**, 329 (1996); G. Chanfray, R. Rapp, and J. Wambach, Phys. Rev. Lett. **76**, 368 (1996); D. K. Srivastava, B. Sinha, and C. Gale, Phys. Rev. C **53**, R567 (1996); K. Haglin, *ibid.* **53**, R2606 (1996); V. Koch and C. S. Song, *ibid.* **54**, 1903 (1996); J. Sollfrank *et al.*, *ibid.* **55**, 392 (1997); C. M. Hung and E. Shuryak, *ibid.* **56**, 453 (1997); R. Baier, M. Dirks, and K. Redlich, Phys. Rev. D **55**, 4344 (1997).

[3] J. V. Steele, H. Yamagishi, and I. Zahed, Phys. Lett. B **384**, 255 (1996); Proceedings of Quark Matter '97, hep-ph/9802256.

[4] J. V. Steele, H. Yamagishi, and I. Zahed, Phys. Rev. D **56**, 5605 (1997).

[5] G. Q. Li, C. M. Ko, and G. E. Brown, Nucl. Phys. **A606**, 568 (1996).

[6] R. Rapp, G. Chanfray, and J. Wambach, Nucl. Phys. **A617**, 472 (1997).

[7] M. Masera for the HELIOS-3 Collaboration, Nucl. Phys. **A590**, 93c (1995).

[8] G. Q. Li and C. Gale, Proceedings of Quark Matter '97, nucl-th/9712076; Phys. Rev. Lett. **81**, 1572 (1998).

[9] C. Gale, in Proceedings of the Third International Conference on Physics and Astrophysics of the Quark-Gluon Plasma,

Jaipur, India, 1997, nucl-th/9706026.
[10] C.-H. Lee, H. Yamagishi, and I. Zahed, hep-ph/9806447.
[11] L. D. McLerran and T. Toimela, Phys. Rev. D **31**, 545 (1985).
[12] H. A. Weldon, Phys. Rev. D **42**, 2384 (1990).
[13] H. Yamagishi and I. Zahed, Ann. Phys. (N.Y.) **247**, 292 (1996); Phys. Rev. D **53**, 2288 (1996).
[14] E. Shuryak, Rev. Mod. Phys. **65**, 1 (1993).
[15] Z. Huang, Phys. Lett. B **361**, 131 (1995).
[16] Particle Data Group, R. M. Barnett *et al.*, Phys. Rev. D **54**, 1 (1996).
[17] C. Bacci *et al.*, Phys. Lett. **86B**, 234 (1979).
[18] J. Siegrist *et al.*, Phys. Rev. D **26**, 969 (1982).
[19] T. H. Hansson, C.-H. Lee, and I. Zahed, ''Thermal Dileptons from a Nonperturbative Quark-Gluon Phase,'' hep-ph/9809440.
[20] P. Wurm, in Proceedings of APCTP Workshop on Astro-Hadron Physics, ''Properties of Hadrons in Matter,'' Seoul, 1997.
[21] G. Q. Li and G. E. Brown (unpublished).
[22] T. H. Hansson and I. Zahed, ''QCD Sum Rules at High Temperature,'' Report No. SUNY-1990 (unpublished); I. Zahed, in *Thermal Field Theories*, edited by H. Ezawa *et al.* (Elsevier, New York, 1991), p. 357; I. Zahed, in *From Fundamental Fields to Nuclear Phenomena*, edited by J. A. McNeil and C. E. Price (World Scientific, Singapore, 1991), p. 238.